




Orbital relaxation length from first-principles scattering calculations

Max Rang  and Paul J. Kelly 

Faculty of Science and Technology and MESA⁺ Institute for Nanotechnology, University of Twente,
P.O. Box 217, 7500 AE Enschede, The Netherlands

 (Received 22 December 2023; revised 10 May 2024; accepted 4 June 2024; published 20 June 2024)

The orbital Hall effect generates a current of orbital angular momentum perpendicular to a charge current. Experiments suggest that this orbital current decays on a long length scale that is of the order of the spin-flip diffusion length or longer. We examine this suggestion using first-principles quantum mechanical scattering calculations to study the decay of orbital currents injected from an orbitally polarized lead into thermally disordered bulk systems of selected transition metals. We find that the decay occurs over only a few atomic layers. On this length scale the orbital current may be converted into a spin current if the spin Hall angle is sufficiently large, as for Pt. In Cu, Cr, and V with small spin Hall angles, the conversion into a spin current is negligible in the bulk and significant conversion only occurs at interfaces.

DOI: [10.1103/PhysRevB.109.214427](https://doi.org/10.1103/PhysRevB.109.214427)

I. INTRODUCTION

The orbital analog of the spin Hall effect (SHE) [1–4], the orbital Hall effect (OHE) [5–8], is predicted to have significantly higher conversion rates than the SHE, in particular for 3d transition metals [9,10]. Experimental results that appear consistent with this theoretical prediction [11–14] invoke long relaxation lengths for the orbital currents. For Ti, for example, relaxation lengths of $50\text{--}60 \pm 15$ nm [8] or 47 ± 11 nm [15] are extracted from magneto-optical Kerr effect (MOKE) and orbital Hall torque (OHT) experiments, respectively; for Cr, MOKE experiments are consistent with a relaxation length of 6.6 ± 0.6 nm [14] while OHT experiments yield a value of 6.1 ± 1.7 nm [16]. Such large values are at variance with the standard picture of orbital quenching in solids according to which orbitally nondegenerate states contain equal amounts of $+m$ and $-m$ character because of time-reversal symmetry [17,18]. Noting that all states in a solid are orbitally nondegenerate at room temperature because thermal disorder eliminates all rotational symmetry, we expect that an orbitally polarized state $|e^{+im\phi}\rangle$ injected into a material at room temperature can only hop to states containing equal amounts of $|e^{+im\phi}\rangle$ and $|e^{-im\phi}\rangle$ character so the orbital polarization is quenched on the length scale of the hopping.

Although it has been argued in a number of recent publications that l_{of} , the orbital analog of the spin-flip diffusion length l_{sf} , is short [19–21], the methods used in these papers were not suitable for making quantitative estimates of l_{of} , in particular in the presence of various types of disorder. It is the purpose of the present work to illuminate the region between theoretical studies on perfectly crystalline and defect-free bulk materials on the one hand and macroscopic experiments on inhomogeneous materials at room temperature on the other, by determining the orbital angular momentum (OAM) relaxation length using quantum mechanical scattering calculations for thermally disordered solids.

II. METHOD

The calculations involve large scattering geometries (thousands of atoms) and take temperature-induced disorder into

account in the adiabatic approximation [22]. The formalism implemented in the Twente Quantum Transport (TQT) [23–26] code considers the disordered material of interest as a scattering region (\mathcal{S}) sandwiched between semi-infinite crystalline left (\mathcal{L}) and right (\mathcal{R}) leads (see Fig. 1). Solution of the time-independent Schrödinger equation by matching the wave functions at the $\mathcal{L}|\mathcal{S}$ and $\mathcal{S}|\mathcal{R}$ interfaces takes the form of a set of inhomogeneous linear equations [28]. The resulting wave function contains all information on the linear response of the system to an external potential [24,29]. On computing the solution in a basis of tight-binding linearized muffin-tin orbitals (TB-LMTOs) [30], we use the continuity equation to extract interatomic (spin and orbital) currents from the wave function [25]. The flux j of the property \hat{X} between atoms P and Q is

$$j_X^{PQ} = \frac{1}{i\hbar} [\langle \Psi_P | \hat{X}_P \hat{H}_{PQ} | \Psi_Q \rangle - \langle \Psi_Q | \hat{H}_{QP} \hat{X}_Q | \Psi_Q \rangle], \quad (1)$$

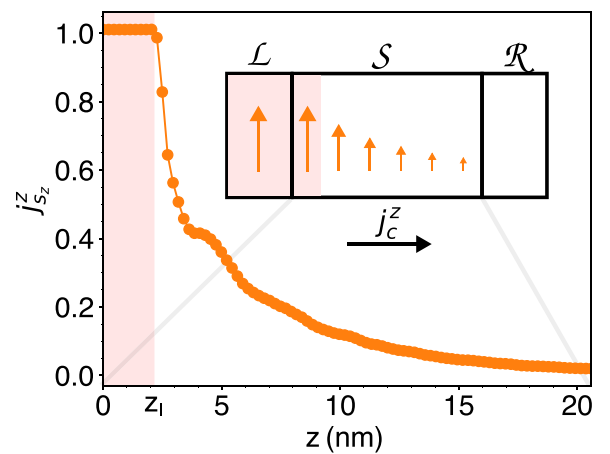


FIG. 1. Exponential decay of a spin-polarized current injected from a ballistic Pt lead into room-temperature (RT) thermally disordered Pt [25]. To visualize the current in the lead, the interface between ballistic (pink) and diffusive Pt is displaced into the scattering region to $z = z_1$ [27].

where $\hat{X} = 1$ leads to an expression for the charge current, $\hat{X} = \hat{S}_\alpha$ yields the spin current polarized in the α direction, and $\hat{X} = \hat{L}_\alpha$ results in the orbital current polarized in the α direction, a current of orbital angular momentum [31]. If the operator \hat{X} is such that $\langle \Psi_P | \hat{X} | \Psi_Q \rangle \neq 0$, this definition of the flux is not well defined since the continuity equation requires local conservation. In particular, we cannot use the definition of the OAM in the so-called ‘‘modern theory of orbital polarization’’ [32–34] to define a current in the scattering approach; instead, we use the atom-centered approximation of the OAM operators to compute OAM currents. Interatomic currents were previously used to compute the spin Hall angle (SHA), spin-flip diffusion length, spin memory loss, and the effect of interface disorder on those parameters [25,35–40].

To construct a spin-polarized current, the (effective [27]) left lead is modified to shift the energy of one of the spin channels so that the Fermi surface becomes completely spin polarized [25]. A charge current injected from the left lead carries a spin current that decays exponentially in the scattering region of thermally disordered bulk diffusive Pt for $z > z_l$ as illustrated in Fig. 1. At room temperature, a value of the spin-flip diffusion length $l_{sf} \approx 5.2$ nm [25,37] can be extracted directly. Constructing a spin-polarized system this way requires introducing a Zeeman term in the Hamiltonian for the left lead, albeit only in the spin degree of freedom

$$\hat{H} = \hat{B} \cdot \hat{S}, \quad (2)$$

where the amplitude of \hat{B} is chosen to completely spin-polarize the Fermi surface.

To compute an orbital relaxation length, we want to inject an orbitally polarized current. To do so, we introduce an orbital Zeeman term into the Hamiltonian for the (effective) left lead,

$$\hat{H} = \hat{B} \cdot \hat{L}, \quad (3)$$

where the choice of amplitude of \hat{B} is not so straightforward as in the spin case. Unlike the spin degrees of freedom which are only coupled weakly through the spin-orbit coupling (SOC), modeled in our case as

$$\hat{H}_{so} = \xi \hat{L} \cdot \hat{S}, \quad (4)$$

the orbital degrees of freedom are much more strongly coupled by the crystal potential so that introducing a significant Zeeman orbital term completely distorts the electronic band structure. The resulting computational setup is sketched in the inset to Fig. 2 and used to inject a current of OAM into thermally disordered, diffusive Pt. The most striking feature of the figure is the very short decay length l_{of} for the OAM current.

III. COMPUTATIONAL DETAILS

The workflow for these calculations is as follows. We begin with a standard density functional theory (DFT) calculation for each transition metal system using the QUESTAAL code [41] with the von Barth–Hedin local density approximation (LDA) functional [42] in combination with a TB-LMTO *spd* basis and a $21 \times 21 \times 21$ \mathbf{k} -point grid. The Kohn-Sham [43] atomic sphere [30] potential is extracted and used to construct the TB-LMTOs in the scattering calculation. The

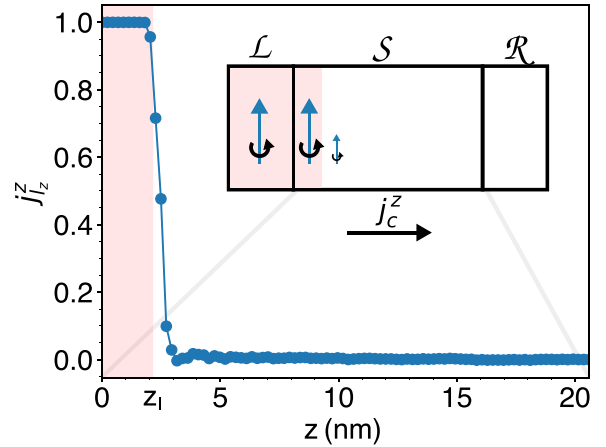


FIG. 2. An orbitally polarized current injected from an orbitally polarized effective left lead [27] decays on a length scale of only a few atomic layers in RT thermally disordered Pt when SOC is not included.

wave-function matching problem [28], which has been shown to be equivalent to the more conventional nonequilibrium Green’s function (NEGF) method [29], is set up and solved in the TQT code. Periodic boundary conditions in the x and y directions (z is the transport direction) require sampling the two-dimensional Brillouin zone with a sufficiently dense \mathbf{k} -point grid. From previous calculations [25], a grid equivalent to 160×160 \mathbf{k} points for a 1×1 unit cell is more than sufficient. Here, we have used a 29×29 \mathbf{k} -point grid with a 5×5 supercell, which is equivalent to 145×145 for a 1×1 unit cell. Thermal disorder is modeled by randomly displacing the atoms from their equilibrium positions in the scattering region (for $z > z_l$) with a Gaussian distribution of displacements. We take multiple configurations of the random disorder and use the average to simulate the thermodynamic mean. In practice, ten configurations is usually sufficient to obtain results uniquely distinguishable from the noise inherent in the random displacements. The root-mean-square disorder parameter is iteratively chosen so that the resistivity of the system is as close to the experimental room-temperature resistivity as desired. ‘‘Room temperature (RT)’’ is defined to be $T = 300$ K.

IV. RESULTS

The orbital current injected into thermally disordered Pt decays very rapidly as seen in Fig. 2. The orbital polarization is unity inside the (effective) left lead [27] but decreases to 2.5% of this value within five atomic layers in diffusive Pt. Fitting an exponential curve to these results is not very meaningful and would result in an ‘‘orbital diffusion length’’ shorter than 1 nm. On plotting the spin and orbital currents together in Fig. 3 for a different, smaller value of $B = 0.05$ Ry with SOC switched on, it can be seen that the orbital current is converted into a spin current within a few layers in disordered Pt. In the few atomic layers where the orbital current decays rapidly, the spin current increases from around 0.06 to 0.08. The polarization of this spin current is not tremendously high,

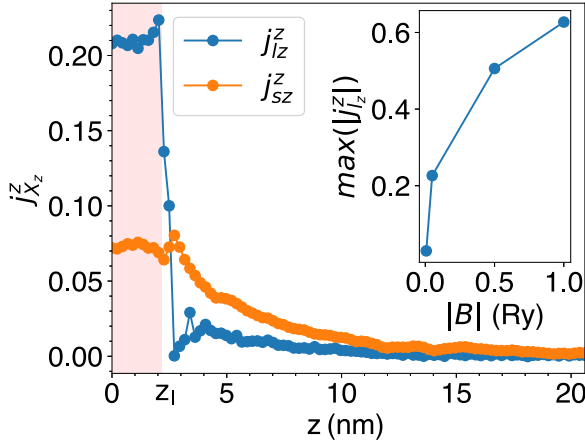


FIG. 3. A current of OAM j_l , orbitally polarized in the z direction (j_{lz}) and injected into RT thermally disordered Pt in the z direction (j_{lz}^z), is converted into a spin current j_s within a few atomic layers after which j_s decays on a length scale consistent with the spin-flip diffusion length of Pt, $l_{\text{Pt}} \equiv l_{\text{sf}}^{\text{Pt}}$. For the orbital Zeeman term in the lead, a value of $B = 0.05$ Ry was used. The inset shows how the degree of orbital polarization depends on the size of the orbital Zeeman splitting in the lead.

around 8% at its peak. It decays on a length scale consistent with the spin-flip diffusion length $l_{\text{Pt}} \equiv l_{\text{sf}}^{\text{Pt}} \approx 5.2$ nm.

The effect of the Pt SOC can be studied by switching it off in the scattering region by setting ξ to zero in (4) (see Fig. 4). The short decay length of the orbital current remains unchanged, of order a few atomic layers. The spin current is zero throughout the scattering region since in the absence of SOC no orbital current is converted into spin current. The sizable difference in the orbital polarization in the lead in the absence of SOC ($\sim 14\%$ without versus $\sim 21\%$ with SOC) comes from the slight change in the band structure when the SOC is turned off. This does not affect the principal result that l_{of} is very short, of the order of a few atomic layers. The same calculation but without thermal lattice disorder and with $B = 0.007$ Ry shows that disorder does not significantly affect

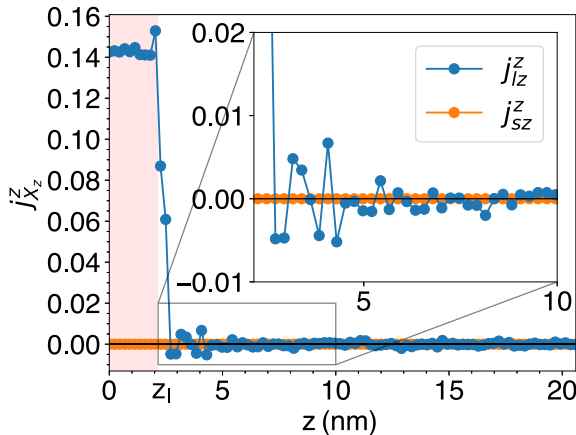


FIG. 4. Same as Fig. 3 but with the SOC switched off. The orbitally polarized current j_l injected into RT thermally disordered Pt decays within a few atomic layers.

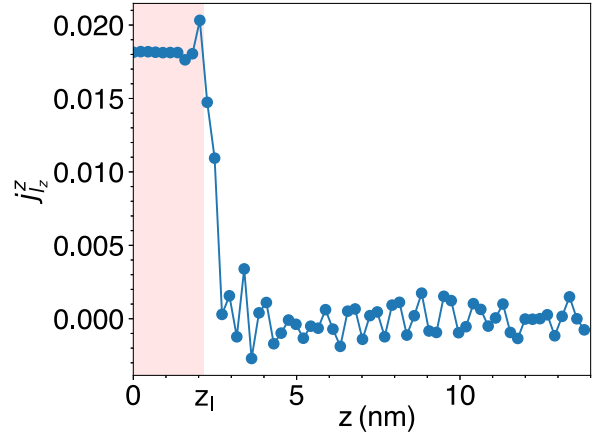


FIG. 5. An orbitally polarized current generated with a value of $B = 0.007$ Ry in the left lead and injected into $T = 0$ K, ordered, Pt decays within a few atomic layers.

l_{of} (Fig. 5) [44]. The fcc structure with $T = 0$ has inversion symmetry while the snapshots of the thermally disordered material used in Fig. 4 do not; we can conclude that inversion symmetry does not play an essential role in the quenching of OAM currents.

An unphysically large value of $B = 40$ Ry in (3) was used to achieve the high degree of orbital polarization seen in Fig. 2 (where the Fermi energy in the lead was shifted to maximize it) and was chosen for illustrative purposes. The short length scale of the decay is unchanged on using a more reasonable value of $B = 0.05$ Ry as in Fig. 3. To test the effect of the orbital Zeeman splitting in the left lead, we calculated the orbital current injection for a number of values of B in Pt. The orbital polarization achievable with these values of $|B|$ is shown in the inset to Fig. 3. For all polarization values, the orbital current decays to less than $1/e$ times its original value within three atomic layers.

As shown in Fig. 6, we observe a short decay length not only for Pt, but also for Cr, V, and Cu. Although different amplitudes of B can produce very different values of the orbital polarization, the orbital current decays to values indistinguishable from the fluctuations arising from disorder sampling within a few atomic layers in all cases. This indicates that the length scale l_{of} does not depend on the orbital Hall conductivity which we find to be large for Cr and V but small for Cu [10].

Even a magnetic field as small as $B = 0.007$ Ry (≈ 100 meV) in (3) polarizes the lead sufficiently to allow the rapid decay of the orbital current injected into V to be clearly registered. In this case, we expect the electronic structure mismatch to be minimal. For the intermediate values of $B = 0.05$ Ry for Cu and $B = 10$ Ry for Cr we find the same behavior; in all cases the orbital current is very short ranged. As in Pt, the orbital current injected into Cr and V generates a spin current through the spin-orbit coupling. However, the conversion rates in Cr and V are so low that the spin currents generated by the orbital-to-spin conversion are practically indistinguishable from the noise inherent in the disordered calculations.

Fitting an exponential curve to extract values for l_{of} for the different materials is not possible. We obtain rough estimates by counting the number of layers over which the polarization

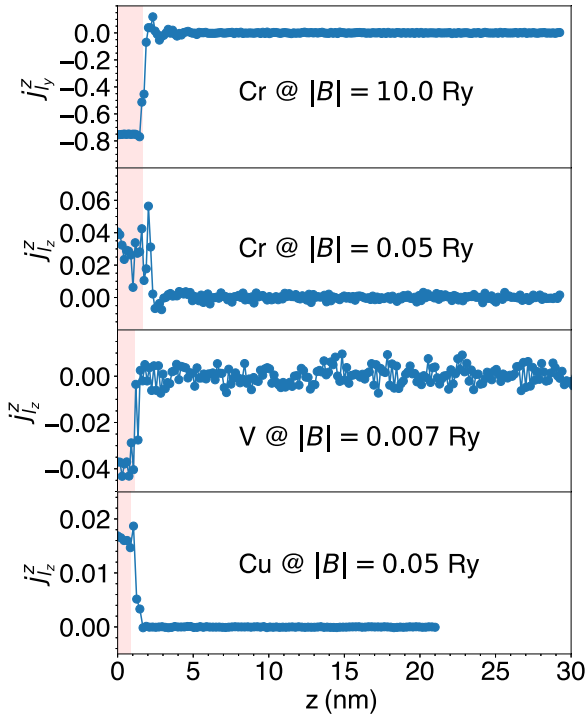


FIG. 6. The orbitally polarized current injected from an orbitally polarized left lead decays on a length scale of only a few atomic layers in thermally disordered Cr, V, and Cu. For Cr, orbitally polarizing fields have been used in the transport direction (J_z^z) and perpendicular to it (J_y^z). The orbital relaxation length is very short in all cases.

drops to $1/e$ times its value in the lead. As shown in Table I, all l_{of} values determined in this way are <1 nm. The range shown for Cr follows from the slight difference between y and z orbital polarizations; in both cases, the value of l_{of} is very small.

V. DISCUSSION

Experiments measuring the orbital Hall effect have been interpreted in terms of long orbital diffusion lengths whereas the results presented here show that the polarization of an orbital current injected into a bulk metal drops off within a few atomic layers. The results for Pt show that the orbital current is converted into a spin current on the same short length scale. One possible explanation of the long length scale extracted

TABLE I. l_{of} values for Pt, Cu, V, and Cr extracted from the decay of orbital polarization inside the scattering region. The number of atomic layers after which the polarization is below the value of $1/e$ times the value in the lead is counted and multiplied by the atomic interlayer distance to obtain an upper bound for l_{of} .

	$1/e$ at layer No.	d (nm) per atomic layer	l_{of} (nm)
Pt	3	0.23	0.6
Cu	2	0.21	0.4
V	3	0.14	0.5
Cr	2–5	0.15	0.3–0.8

from experiment is that what is being observed is the long l_{sf} over which the spin current resulting from the injected orbital current decays rather than the orbital current itself.

Exactly how the orbital current might be converted into a spin current in systems containing the light elements Cr and Ti is unclear. One possible explanation is that there is some orbital-to-spin conversion taking place at an interface or surface facilitated by the reduced symmetry of the interface. Another possibility is that a large spin Hall current may be generated directly at the interface where the $3d$ materials simply serve to facilitate symmetry breaking by being different from the ferromagnetic material with which they are interfaced [35]. Lastly, we note that large spin Hall angles are theoretically predicted in late $3d$ metals where the reduced $3d$ bandwidth compensates for the reduced SOC [45–48]; this is expected to greatly complicate the interpretation of experiments performed on bilayers [48].

Though the precise mechanism may be dependent on the experiment being performed, it is well known that the effect of SOC is greatly enhanced by the symmetry lowering at an interface. The results presented here show that the orbital current can be converted into a spin current within a few atomic layers and this process could be compatible with an interface-mediated mechanism. One conclusion we can draw from the results presented here is that only a few atomic layers are needed to convert almost all of the orbital current into a spin current and a thick slab of orbital-to-spin conversion material may not be needed.

Our finding that l_{of} is very short is not necessarily bad news. The origin of the torque exerted by injecting a spin or orbital current from a nonmagnetic into a magnetic material is largely a matter of interpretation; for example, no change has to be made to electronic-structure-based computer codes that calculate spin-orbit torque (SOT) to include the OHE; it is included automatically. The important insight from OHE studies is that the search for efficient SOT need not be restricted to heavy metals with large spin-orbit coupling, the reduced bandwidth and frequently large state density at the Fermi energy of $3d$ elements being frequently more important [45–48]. One consequence of a very short l_{of} is that the orbital Hall conductivity is not a useful figure of merit in the search for better SOT materials. Another is that because the SOT is essentially a property of an A|B interface, it cannot be factored into separate A and B parts.

VI. CONCLUSION

By computing the decay of orbital currents injected from an orbitally polarized lead, we have shown that the orbital relaxation length in transition metals is as short as might be expected from classical orbital quenching arguments. In all cases studied here, the orbital polarization decays to less than $1/e$ times its injected value within less than a nanometer. It does not matter if the polarization is small or large. The decay length does not depend on the spin Hall angle (l_{of} is short for both Pt with a large SHA and for Cu with a negligible SHA) or the orbital Hall angle (l_{of} is short for V and Cr as well as for Cu). The conversion of the orbital current into a spin current does significantly depend on the spin Hall angle, as expected. These results contradict the interpretation of

experimental findings in terms of significantly longer length scales. One possible explanation is that the experiments are actually measuring the spin-flip diffusion length instead. In the case of Pt, we have shown how the injected orbital current is converted into a spin current within a few layers after which it decays as we expect for the spin current.

ACKNOWLEDGMENTS

This work was sponsored by NWO Domain Science for the use of supercomputer facilities. We acknowledge discussing the role of thermal disorder with Sergei Urazhdin and Thierry Valet.

- [1] M. I. Dyakonov and V. I. Perel, Current-induced spin orientation of electrons in semiconductors, *Phys. Lett. A* **35**, 459 (1971).
- [2] M. I. D'yakonov and V. I. Perel, Possibility of orienting electron spins with current, *Zh. Eksp. Teor. Fiz.* **13**, 657 (1971) [*JETP Lett.* **13**, 467 (1971)].
- [3] J. E. Hirsch, Spin Hall effect, *Phys. Rev. Lett.* **83**, 1834 (1999).
- [4] S. O. Valenzuela and M. Tinkham, Direct electronic measurement of the spin Hall effect, *Nature (London)* **442**, 176 (2006).
- [5] T. Tanaka, H. Kontani, M. Naito, T. Naito, D. S. Hirashima, K. Yamada, and J. Inoue, Intrinsic spin Hall effect and orbital Hall effect in $4d$ and $5d$ transition metals, *Phys. Rev. B* **77**, 165117 (2008).
- [6] H. Kontani, T. Tanaka, D. S. Hirashima, K. Yamada, and J. Inoue, Giant orbital Hall effect in transition metals: Origin of large spin and anomalous Hall effects, *Phys. Rev. Lett.* **102**, 016601 (2009).
- [7] D. Go, D. Jo, C. Kim, and H.-W. Lee, Intrinsic spin and orbital Hall effects from orbital texture, *Phys. Rev. Lett.* **121**, 086602 (2018).
- [8] Y.-G. Choi, D. Jo, K.-H. Ko, D. Go, K.-H. Kim, H. G. Park, C. Kim, B.-C. Min, G.-M. Choi, and H.-W. Lee, Observation of the orbital Hall effect in a light metal Ti, *Nature (London)* **619**, 52 (2023).
- [9] D. Jo, D. Go, and H.-W. Lee, Gigantic intrinsic orbital Hall effects in weakly spin-orbit coupled metals, *Phys. Rev. B* **98**, 214405 (2018).
- [10] L. Salemi and P. M. Oppeneer, First-principles theory of intrinsic spin and orbital Hall and Nernst effects in metallic monoatomic crystals, *Phys. Rev. Mater.* **6**, 095001 (2022).
- [11] G. Sala and P. Gambardella, Giant orbital Hall effect and orbital-to-spin conversion in $3d$, $5d$, and $4f$ metallic heterostructures, *Phys. Rev. Res.* **4**, 033037 (2022).
- [12] A. Rothschild, N. Am-Shalom, N. Bernstein, M. Meron, T. David, B. Assouline, E. Frohlich, J. Xiao, B. Yan, and A. Capua, Generation of spin currents by the orbital Hall effect in Cu and Al and their measurement by a Ferris-wheel ferromagnetic resonance technique at the wafer level, *Phys. Rev. B* **106**, 144415 (2022).
- [13] J. Zhang, H. Xia, X. Zhang, Z. Yan, Y. Zhai, J. Chi, H. Xu, Y. Zuo, and L. Xi, The giant orbital Hall effect in Cr/Au/Co/Ti multilayers, *Appl. Phys. Lett.* **121**, 172405 (2022).
- [14] I. Lyalin, S. Alikhah, M. Berritta, P. M. Oppeneer, and R. K. Kawakami, Magneto-optical detection of the orbital Hall effect in chromium, *Phys. Rev. Lett.* **131**, 156702 (2023).
- [15] H. Hayashi, D. Jo, T. Gao, S. Haku, Y. Mokrousov, H.-W. Lee, and K. Ando, Observation of long-range orbital transport and giant orbital torque, *Commun. Phys.* **6**, 32 (2023).
- [16] S. Lee, M.-G. Fang, D. Go, D. Kim, J.-H. Kang, T. Lee, G.-H. Lee, J. Hang, N. J. Lee, Y. Mokrousov, S. Kim, K.-J. Kim, K.-J. Lee, and B.-G. Park, Efficient conversion of orbital Hall current to spin current for spin-orbit torque switching, *Commun. Phys.* **4**, 234 (2021).
- [17] P. Mohn, in *Magnetism in the Solid State: An Introduction*, edited by M. Cardona, P. Fulde, K. von Klitzing, and H.-J. Queisser, Springer Series in Solid-State Sciences (Springer, Berlin, Heidelberg, 2003), Vol. 134.
- [18] M. Tinkham, *Group Theory and Quantum Mechanics*, Dover Books on Chemistry (Dover, New York, 2003).
- [19] L. Salemi, M. Berritta, and P. M. Oppeneer, Quantitative comparison of electrically induced spin and orbital polarizations in heavy-metal/ $3d$ -metal bilayers, *Phys. Rev. Mater.* **5**, 074407 (2021).
- [20] K. D. Belashchenko, G. G. Baez Flores, W. Fang, A. A. Kovalev, M. van Schilfgaarde, P. M. Haney, and M. D. Stiles, Breakdown of the drift-diffusion model for transverse spin transport in a disordered Pt film, *Phys. Rev. B* **108**, 144433 (2023).
- [21] S. Urazhdin, Symmetry constraints on orbital transport in solids, *Phys. Rev. B* **108**, L180404 (2023).
- [22] Y. Liu, Z. Yuan, R. J. H. Wesselink, A. A. Starikov, M. van Schilfgaarde, and P. J. Kelly, Direct method for calculating temperature-dependent transport properties, *Phys. Rev. B* **91**, 220405(R) (2015).
- [23] K. Xia, M. Zwierzycki, M. Talanana, P. J. Kelly, and G. E. W. Bauer, First-principles scattering matrices for spin-transport, *Phys. Rev. B* **73**, 064420 (2006).
- [24] A. A. Starikov, Y. Liu, Z. Yuan, and P. J. Kelly, Calculating the transport properties of magnetic materials from first-principles including thermal and alloy disorder, non-collinearity and spin-orbit coupling, *Phys. Rev. B* **97**, 214415 (2018).
- [25] R. J. H. Wesselink, K. Gupta, Z. Yuan, and P. J. Kelly, Calculating spin transport properties from first principles: Spin currents, *Phys. Rev. B* **99**, 144409 (2019).
- [26] R. S. Nair and P. J. Kelly, Fully resolved currents from quantum transport calculations, *Phys. Rev. B* **103**, 195406 (2021).
- [27] Because of how currents are extracted from the scattering wave functions [25], $j(z)$ is not calculated in the leads. To visualize $j(z)$ in the left-hand lead (\mathcal{L}), the $\mathcal{L}|S$ interface is artificially shifted into the scattering region to $z = z_l$. The region $z < z_l$ where the magnetic field \hat{B} in (2) and (3) is nonzero and there is no thermal disorder is indicated in the figures by pink shading. For simplicity, this effective lead will be referred to as the lead and the part of the scattering region $z > z_l$ will be referred to as the scattering region.
- [28] T. Ando, Quantum point contacts in magnetic fields, *Phys. Rev. B* **44**, 8017 (1991).
- [29] P. A. Khomyakov, G. Brocks, V. Karpan, M. Zwierzycki, and P. J. Kelly, Conductance calculations for quantum wires and

- interfaces: Mode matching and Green functions, *Phys. Rev. B* **72**, 035450 (2005).
- [30] O. K. Andersen and O. Jepsen, Explicit, first-principles tight-binding theory, *Phys. Rev. Lett.* **53**, 2571 (1984); O. K. Andersen, O. Jepsen, and D. Glötzel, *Canonical description of the band structures of metals*, in *Proceedings of the International School of Physics 'Enrico Fermi'; Course LXXXIX. Highlights of Condensed-Matter Theory*, Varenna, Italy, edited by F. Bassani, F. Fumi, and M. P. Tosi (North-Holland, Amsterdam, 1985), pp. 59–176; O. K. Andersen, Z. Pawłowska, and O. Jepsen, Illustration of the linear-muffin-tin-orbital tight-binding representation: Compact orbitals and charge density in Si, *Phys. Rev. B* **34**, 5253 (1986).
- [31] For convenience, we measure the charge density in units of the electron charge $-e$ (where e is a positive quantity), the spin density in units of $\hbar/2$, and the orbital density in units of \hbar so they all become particle densities and the fluxes become particle fluxes.
- [32] T. Thonhauser, D. Ceresoli, D. Vanderbilt, and R. Resta, Orbital magnetization in periodic insulators, *Phys. Rev. Lett.* **95**, 137205 (2005).
- [33] T. P. Cysne, S. Bhowal, G. Vignale, and T. G. Rappoport, Orbital Hall effect in bilayer transition metal dichalcogenides: From the intra-atomic approximation to the Bloch states orbital magnetic moment approach, *Phys. Rev. B* **105**, 195421 (2022).
- [34] A. Pezo, D. Garcia Ovalle, and A. Manchon, Orbital Hall effect in crystals: Interatomic versus intra-atomic contributions, *Phys. Rev. B* **106**, 104414 (2022).
- [35] L. Wang, R. J. H. Wesselink, Y. Liu, Z. Yuan, K. Xia, and P. J. Kelly, Giant room temperature interface spin Hall and inverse spin Hall effects, *Phys. Rev. Lett.* **116**, 196602 (2016).
- [36] K. Gupta, R. J. H. Wesselink, R. Liu, Z. Yuan, and P. J. Kelly, Disorder dependence of interface spin memory loss, *Phys. Rev. Lett.* **124**, 087702 (2020).
- [37] R. S. Nair, E. Barati, K. Gupta, Z. Yuan, and P. J. Kelly, Spin-flip diffusion length in $5d$ transition metal elements: A first-principles benchmark, *Phys. Rev. Lett.* **126**, 196601 (2021).
- [38] K. Gupta, R. J. H. Wesselink, Z. Yuan, and P. J. Kelly, Spin transport at finite temperatures: A first-principles study for ferromagnetic|nonmagnetic interfaces, *Phys. Rev. B* **104**, 205426 (2021).
- [39] K. Gupta, R. Liu, R. J. H. Wesselink, Z. Yuan, and P. J. Kelly, Calculating interface transport parameters at finite temperatures: Nonmagnetic interfaces, *Phys. Rev. B* **106**, 115425 (2022).
- [40] R. Liu, K. Gupta, Z. Yuan, and P. J. Kelly, Calculating the spin memory loss at Cu|metal interfaces from first principles, *Phys. Rev. B* **106**, 014401 (2022).
- [41] D. Pashov, S. Acharya, W. R. Lambrecht, J. Jackson, K. D. Belashchenko, A. Chantis, F. Jamet, and M. van Schilfgaarde, Questaal: A package of electronic structure methods based on the linear muffin-tin orbital technique, *Comput. Phys. Commun.* **249**, 107065 (2020).
- [42] U. von Barth and L. Hedin, A local exchange-correlation potential for the spin-polarized case: I, *J. Phys. C: Solid State Phys.* **5**, 1629 (1972).
- [43] W. Kohn and L. J. Sham, Self-consistent equations including exchange and correlation effects, *Phys. Rev.* **140**, A1133 (1965).
- [44] Our interpretation of the very small value of l_{of} in terms of orbital quenching and time-reversal symmetry becomes more complicated at $T = 0$ K when orbital degeneracies occur. Nevertheless, the numerical calculations are easily performed in the absence of thermal disorder and l_{of} does not change appreciably. Thus thermal disorder is not responsible for the quenching of orbital currents.
- [45] K. Gupta, Disentangling interfaces and bulk in spin transport calculations, Ph.D. thesis, University of Twente, 2019, doi:10.3990/1.9789036547765.
- [46] V. P. Amin, J. Li, M. D. Stiles, and P. M. Haney, Intrinsic spin currents in ferromagnets, *Phys. Rev. B* **99**, 220405(R) (2019).
- [47] R. S. Nair, Spin-orbit-coupling induced lateral spin transport from first principles, Ph.D. thesis, University of Twente, 2021, doi:10.3990/1.9789036552110.
- [48] M. Rang, Influence of disorder, surfaces and interfaces in the spin and orbital Hall effects via first-principles quantum mechanical scattering calculations, Ph.D. thesis, University of Twente, 2024.